

Energetic, electronic and magnetic properties of Mn dimers on GaAs reconstructed (001) surfaces

Magdalena Popielska*

Institute of Theoretical Physics, University of Warsaw, Pasteura 5, PL-02-093 Warszawa, Poland,

Cezary Śliwa

*Institute of Physics, Polish Academy of Sciences,
al. Lotników 32/46, PL-02-668 Warszawa, Poland,*

Jacek A. Majewski

Institute of Theoretical Physics, University of Warsaw, Pasteura 5, PL-02-093 Warszawa, Poland.

(Dated: December 9, 2024)

We present a computational study of substitutional Mn pairs on the (001) GaAs reconstructed surfaces in diluted regime, in the framework of the density functional theory. We focus on the energetic, magnetic, and electronic properties of such systems. We have demonstrated that the energy of the system strongly depends on the position, orientation, and the distance between the Mn-atoms. The most preferential energetically position of Mn-pair is the nearest neighbor position (NN, Mn-dimer), independently of the reconstruction pattern studied in this paper. In case of NN Mn-pairs we find that Mn-pairs have preferential build-up orientations [110] or [1-10], which depends on the reconstruction used in the calculations. Our results also demonstrate the mechanism of the magnetic ordering depends on the Mn-pair orientation. In the case of the Mn-dimer along the [110] crystallographic direction exhibits ferromagnetic alignment of spins, whereas the Mn-dimers along [1-10] direction are mostly anti-ferromagnetically aligned. Moreover, in the ferromagnetically aligned Mn-pairs the extra states appear in the valence band just above the Fermi level. We identify them with the acceptor holes states, proving that the surface ferromagnetism in this prototype DMS can be explained in terms of the p-d Zener model.

I. INTRODUCTION

Nowadays, the epitaxially grown semiconducting magnetic films like (Ga,Mn)As have attracted great deal of attention, mostly due to its considerable properties for spintronic applications. It has been experimentally shown that its properties depend strongly on how the magnetic ions are incorporated into the host, in particular, interstitial Mn-ions can reduce the Curie temperature or the hole concentration, and hence hinder ferromagnetism. Moreover, the existence of the preferential build-up direction of Mn dimers along the [-110] direction onto GaAs(001) surface results in a bulk uniaxial magnetic anisotropies (in-plane and out-of-plane) has been theoretically shown by the authors [1]. The uniaxial magnetic anisotropy in systems is of crucial importance to design novel spintronics devices [2]. Furthermore, it has been reported that a single atom substitution technique, with spectroscopic imaging in a scanning tunneling microscope (STM), opens a new way to manipulate atom by atom at the surface [3]. To control the location of Mn in (Ga,Mn)As, it is crucial to understand the initial incorporation processes of Mn in GaAs host.

So far, theoretical approaches reported, by using the self-consistent Hückel method and a cluster model, that the Mn-atoms prefers to be substituted at the surface

Ga-atom instead of being adsorbed above it [4]. Recently, the DFT calculations demonstrated, under the non-equilibrium conditions of growth (by identifying the reactions pathways), that the interstitial Mn is easily incorporated beneath the As-As dimer on the GaAs(001) surface [5]. Then Zhang et al. [6] have showed that the stability of several types of structures induced by the Mn adsorption depends on the stoichiometry of the surface composition. Very recently the combined DFT calculations (under the equilibrium conditions of growth) and experimental works have demonstrated [7] that Mn-atoms prefer to substitute Ga-sites at a subsurface layer under the As-rich conditions for GaAs (001) oriented surface, whereas interstitial sites are preferable under Ga-rich conditions. Moreover, the preferable incorporation of Mn-ions in the substitutional site in GaAs under As-rich conditions had been predicted before by Zunger [8]. Therefore, we have performed extensive studies of all possible non-equivalent substitutional positions of the Mn pairs onto GaAs (001) reconstructed surfaces: (2×1) , $\beta(2 \times 4)$, $\beta 2(2 \times 4)$, under As-rich conditions.

In addition, the magnetism of differently oriented surfaces in general and theirs reconstructions in particular, are only very weakly understood quantitatively up to now. Strandberg et al. [9] studied the Mn pairs at different crystallographic orientations at (110) GaAs surface, by using the Kinetic Tight Binding model. They showed that the long-range interactions are anisotropic in terms of orientations and distances between the Mn-pairs. They also obtained that the magnetic ions prefer

* Magdalena.Birowska@fuw.edu.pl

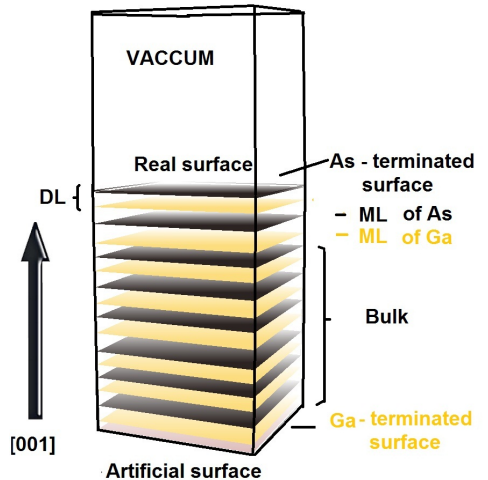
to be ferromagnetically arranged. Fhokrum Islam et. al. [10] by used of the Density Functional method showed the anisotropic character of the effective exchange constant for the Mn pairs differently oriented at (110) surface. Both papers studied the most common cleaved surface employed in cross sectional STM studies, although this is not the most common GaAs growth surface, which is the (001). In the literature there is a lack information about the exchange interaction between the magnetic ions (in dilute regime) onto the experimentally observed reconstructed GaAs (001) surfaces. Moreover, the surface reconstruction plays an important role in the homo- and heteroepitaxy on GaAs(001).

Detailed knowledge of the magnetic interactions at the reconstructed surfaces is essential in fabricating new high speed spintronics devices. Therefore in this work we focus on magnetic properties of substitutional positions of Mn dimers onto the differently reconstructed GaAs (001) surfaces in diluted case. Moreover, we report the role of the surface reconstruction in the Mn incorporation process. We also examine the energetic properties and stability of Mn-GaAs surfaces.

II. COMPUTATIONAL DETAILS

The calculations are performed using DFT [11, 12] within the L(S)DA+U approach, and parameterization provided by Ceperly and Alder (CA) [13] of the exchange-correlation functional as is implemented in SIESTA code [14]. The electron ion-core interactions are represented by norm-conserving pseudopotentials of the Troullier-Martins type [15] with non-linear core corrections [16]. The electron wave-functions are expanded into a flexible multiple centered atom basis set of numerical atomic orbitals [17]. Our calculations use double- ζ for the s and p shells of any element and a triple- ζ basis set for the Mn $3d$ shell. The cutoffs of 300 Ry and 30 \AA are used for the real and reciprocal space meshes. These parameters have been chosen providing sufficient accuracy of the surface energy, being not worth than 0.05 meV/\AA^2 . For L(S)DA+U calculations, we adopted the value of the U parameter equal to 4.5 eV for Mn $3d$ states, which is in perfect agreement with the previous photoemission data [18], and consistent with previous L(S)DA+U calculations for the bulk [19, 20].

In order to get a set of reasonably optimized parameters steering the computational run of the surface calculations, we have made the careful tests. That guarantees simultaneously the required accuracy and high efficient of very demanding computations. We attempt to evaluate the systematic errors of the performed calculations. In particular, we are interested in energetics of the surface calculations, therefore, the convergence in terms of the surface free energy is checked. Our calculation accuracy of the surface free energy is not smaller than $0.37 \text{ [meV/\AA}^2]$, which is quite accurate if one compares this value with the typical values of the surface energy for



(color online)

FIG. 1. The schematic diagram of the supercell used in the calculations. The supercell consists of 8 DL of As-Ga. Each monolayer contains 16 atoms. The artificial surface denotes the surface with saturated dangling bonds, which mimics the bulk type of bindings.

GaAs(001), which are in between 40 to 100 $[\text{meV/\AA}^2]$ [21].

A. Model of a surface

In order to investigate the physical properties of substitutional isolated Mn-pairs on the GaAs(001) surfaces, we used supercell geometry and construct the slab system as it is presented in Fig. 1. To model GaAs (001) surface, 8 double As-Ga layers (DLs) lying in the (001) crystallographic plane are used. The GaAs crystal is represented by a standard zinc blende (zb) cell with calculated lattice parameter equals to 5.639 \AA , and it is in good agreement with experimental value 5.648 \AA [22]. If the slab is not thick enough, the dangling bond states on the two sides of the slab might interact with each other and give rise to artificial charge transfer from top surface of the slab to its bottom. To avoid this effect and decouple the two sides of the slab and we saturate the dangling bonds from the bottom side of the slab by a monolayer of pseudo-Hydrogen atoms with fractional charge equal to $Z = 1.25$. Each of the Ga-atom is saturated by 2 pseudo-atoms, to mimic the bulk types of bonds. In order to simulate independent crystal surface 16 \AA of vaccum is added, with the *slab dipole correction* and *simulate doping* options enabled as it is implemented in SIESTA code [14].

We consider experimentally observed reconstructed GaAs (001) surfaces under As-rich conditions: $\beta(2 \times 4)$ [23], $\beta_2(2 \times 4)$ [24–27], and also theoretically proposed (2×1) reconstruction[28] [29], which are presented in Fig. 2. All of the atoms in pure surfaces are fully relaxed until the maximal force on each of the atom reaches the

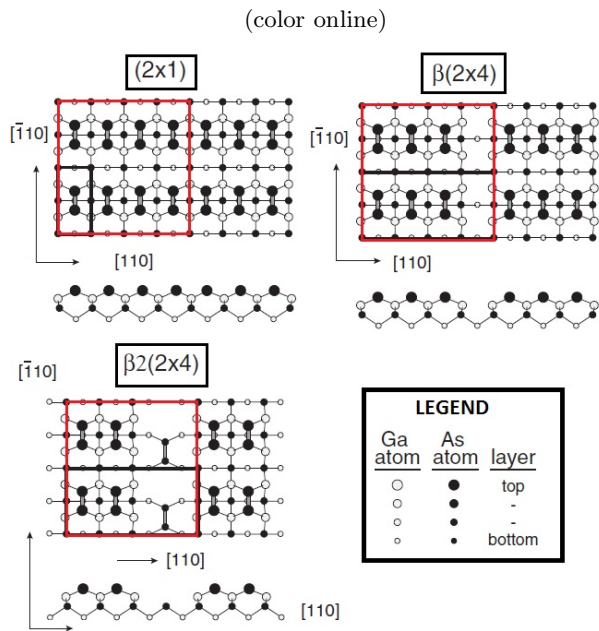


FIG. 2. The schematic diagrams of GaAs (001) reconstructed surfaces under As-rich conditions used in this work. On the surface As-As dimerization along $[-110]$ direction is clearly visible. Four monolayers from the top of the slab are shown. Positions in the uppermost atomic layers are indicated by larger symbols. The black and white balls indicate the arsenic and gallium atoms. The rectangular, red line denotes the lateral supercell chosen for the calculations.

value of $0.02 \text{ eV}/\text{\AA}$. These surfaces are our inputs for further calculations.

To investigate the physical properties of isolated Mn-pairs (it models properly diluted case), we substitute two Ga-atoms by two Mn-atoms at the top most monolayer of Ga-atoms at pure GaAs (001) reconstructed surfaces. Our simulated supercell contains around 280 atoms, each of the monolayer comprises 16 atoms, making the Mn-coverage of the layer equal to $1/8$. The surface area corresponds to lateral cell of the dimensions $16\text{\AA} \times 16\text{\AA}$. During the optimization procedure 6 ML from the top of the slab are fully relaxed, whereas the bottom of the slab is fixed to reflect the bulk character of the supercell.

III. RESULTS

This section is organized as follows. We divided our results into two main parts: Energetics and the Magnetic Properties.

A. Energetics

In the section, we focus on structural and energetic properties in the standpoint of the different possible incorporation of Mn-pairs which are embedded onto

cationic sublattice into the given reconstructed GaAs surface (001): (2×1) , $\beta(2 \times 4)$, and $\beta 2(2 \times 4)$. Then, we compare the effects introduced by these reconstructions and we define the stability of such a structures.

1. Reconstruction (2×1)

We start by considering all non-equivalent positions of Mn-pairs (two Mn-ions per cell), oriented along different crystalline directions and at various separations of Mn-pairs, substituted onto cationic sublattice of Ga-atoms at the optimized (2×1) reconstructed GaAs(001) surface, as it shown in Fig. 3 (A), where the position of one Mn-atom is kept fixed (at position 0 in Fig. 3 (A)), whereas the position of the second atom is varied along different crystallographic directions at the (001) surface.

At the (2×1) surface, the lowest energy is for the Mn-pair occupying the nearest neighbors positions, as it evident from Fig. 3 (B). Moreover, the total energy increases with the distance between the Mn-atoms constituting the Mn-pair. These results suggest that Mn-atoms prefer to form the pairs at the surface. Furthermore, the energy strongly depends on the orientation of Mn-pair at the surface for the equally spaced Mn-ions (see Fig. 3(B)). For two different orientation at the surface and considered Mn-pair arrangements, the energies vary within 0.3 eV , which indicates that the thermal energy at room temperature cannot change most of the position of atoms at the surface. This result suggests that the local environment around the Mn-pair has significant influence on the incorporation of Mn-atoms. Let us now examine this effect deeper, in the standpoint of the most energetically preferable nearest neighbor positions (NN).

To investigate it, we place Mn-pair on the pure (2×1) GaAs surface (non-optimized case) and compare it with the case when the atoms are relaxed up to sixth ML down from the top of the As-terminated surface (optimized case). In Fig. 4, it is clearly seen that for non-optimized case the lower total energy is when the Mn-pair is placed along $[1-10]$ crystallographic direction, whereas local changes of geometry around Mn-pair (optimized case) change the preferential energetically direction to $[110]$, independently of the method (LDA or L(S)DA+U), used in the calculations.

It is worth to point out now that when we place Mn-pair along $[110]$ crystallographic direction, the symmetry is lowered to C_v in comparison to pure (2×1) GaAs(001) surface (where it is C_{2v}), whereas Mn-pair placed along the $[1-10]$ direction doesn't change the symmetry of the layer. As a consequence, we have noticed stronger relaxation of the atoms around the Mn-pair along $[110]$ direction, than for the Mn-pair along the $[1-10]$ direction.

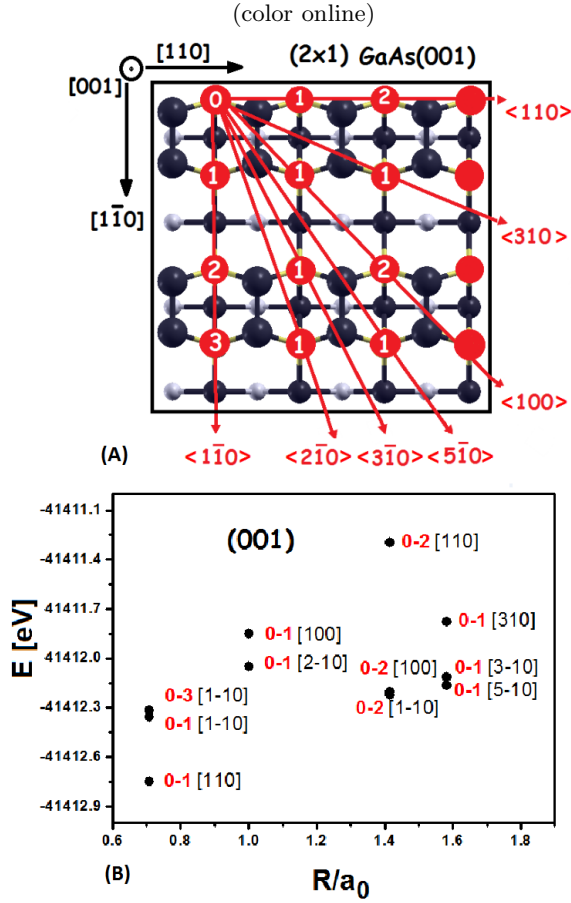


FIG. 3. (A) All non-equivalent positions of Mn-pair on the (2×1) reconstructed (001) surface. The two Mn-atoms, replacing Ga-atoms (red spheres), are marked 0 (first Mn-atom) and 1,2,3 (second Mn-atom), e.g. 0-3 [1-10] denotes that the Mn-pair is along [1-10] crystallographic direction, where Mn-atoms constituting the pair sit on 0 and 3 position as is depicted on panel (A). All equivalent symmetry directions $\langle \dots \rangle$ have been chosen in direct cubic coordinates [...], in such a way that all Mn-pairs appear in (001) plane. Positions of the atoms in the uppermost monolayers are indicated by larger symbols. (B) The total energy given in eV per supercell versus the distance between Mn-pairs, placed along indicated in square parenthesis crystallographic directions. The lowest energy is when the Mn-ions are at the nearest neighbor position.

2. Reconstruction $\beta(2 \times 4)$

We start the discussion with a survey of possible placements of the Mn-pairs on the $\beta(2 \times 4)$ GaAs (001) surface (see Fig. 5). In the chosen supercell of C_{2v} symmetry the [110] and [1-10] directions are non-equivalent. Along each of these directions we can place the nearest neighbor Mn-pair on four equivalent ways on the cationic sublattice. They are, 1 & 2, 5 & 6, 9 & 10, 13 & 14 and 1 & 5, 2 & 6, 9 & 13, 10 & 14 for [110] and [1-10] directions, respectively.

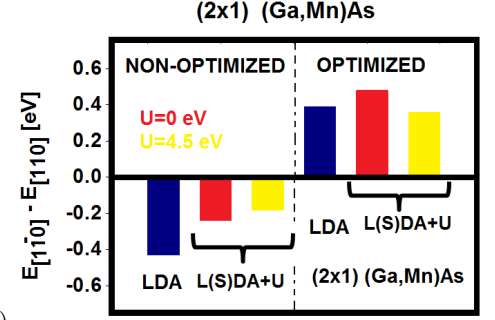


FIG. 4. The energy difference between Mn-pair along the [1-10] and [110] directions of (2×1) GaAs(001) surface, for the following computational schemes: (i) spin unpolarized LDA, and (ii) L(S)DA+U for $U = 0$ eV, i.e., standard L(S)DA (indicated with red color), and $U = 4.5$ eV (indicated with yellow). In the L(S)DA, the difference is between the magnetic ground states of Mn-pair along [1-10] and at [110] directions. For non-optimized geometry of the slab, the ground state is when the Mn-pair is situated along [1-10] direction, whereas the optimization changes the preferential direction to the [110] direction.

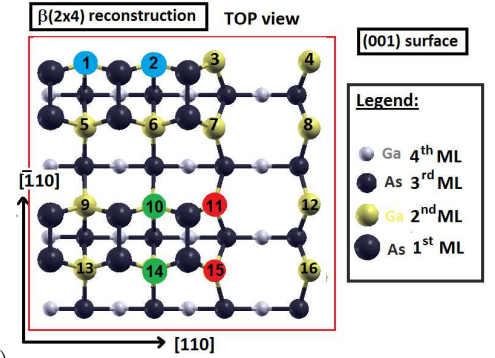


FIG. 5. Positions of the Mn-pair at the $\beta(2 \times 4)$ reconstructed surface. The most energetically favorable positions of the Mn-pair are indicated by the blue color (numbered 1 & 2, which is the same for both L(S)DA and L(S)DA+U approaches), and for the [1-10] crystallographic direction with green for L(S)DA (numbered 10 & 14) and with red for L(S)DA+U (numbered 11 & 15) schemes. The all other possible cationic positions where the Mn-atoms could be accommodated are indicated in yellow and also numbered. Positions of the As-atoms are denoted with big black dots and small grey dots, for the highest and deeper As-layers, respectively.

However, along the [110] and [1-10] directions we can place Mn nearest neighbor pairs also in non-equivalent positions, such as 1 & 2, 2 & 3, 3 & 4, along [1-10] and 6 & 10, 7 & 11, 10 & 14, 11 & 15 for Mn-pair along [1-10].

From Fig. 5, one can also deduce the positions of the Mn-pairs with longer than nearest neighbor distances between Mn-atoms. We have performed calculations for all non-equivalent positions of the Mn-pairs. It turns out that the pairs with Mn-atoms being the nearest neighbors are energetically preferable in comparison of the config-

TABLE I. The ground state energies for all of the non-equivalent incorporations of the Mn-dimer at the nearest neighbor positions at the (001) $\beta(2 \times 4)$ surface. The Mn-pair positions are explained in Fig. 5. The displaced energies are the differences $\Delta E = E_{tot}^{slab, Mn}(MS) - E_{tot}^{slab, pure}$, given in eV per supercell. MS indicates the alignment of Mn magnetic moments, MS = FM, or AFM, and the $E_{tot}^{slab, pure} = -39813.12$ eV per supercell which contains 284 atoms. The results are obtained employing standard L(S)DA and L(S)DA+U (for $U = 4.5$ eV) approaches.

$\beta(2 \times 4)$ position	$\Delta E_{L(S)DA}$		$\Delta E_{L(S)DA+U}$ ($U = 4.5$ [eV])	
	E_{FM}	E_{AFM}	E_{FM}	E_{AFM}
[110] 1 & 2	-737.743	-737.448	-743.792	-743.555
[110] 2 & 3	-737.582	-737.456	-743.765	-743.666
[110] 3 & 4	-737.561	-737.413	-743.756	-743.636
[1-10] 6 & 10	-737.415	-737.455	-743.521	-743.582
[1-10] 7 & 11	-737.095	-737.053	-743.443	-743.430
[1-10] 10 & 14	-737.539	-737.557	-743.627	-743.623
[1-10] 11 & 15	-737.195	-737.318	-743.605	-743.697

urations with larger distances between the Mn-atoms.

However, the relative energy differences among this class of configurations are dependent on the alignment of magnetic moments of the Mn-atoms (FM or AFM). This is illustrated in Tab. I, where the difference of the total energies of slab with Mn-pair and the pure slab (i.e., without Mn-pair) are given for the L(S)DA and L(S)DA+U method.

Note that the total energy of the pure slab can be considered as a reference energy. This energy is identical for the L(S)DA and L(S)DA+U case, since for the atoms in the pure slab (As, Ga, H) the Hubbard term U is always taken as zero.

The energies of all non-equivalent Mn-pair arrangements (with Mn-atoms being the nearest neighbors) are presented in Tab. I.

Among the NN Mn-pairs placed along [110] direction, the lowest total energy is for FM Mn-spin arrangements and the Mn-pairs 1 & 2 (see Fig. 5, where this pair is indicated in blue). This is true for both L(S)DA and L(S)DA+U approaches. Among all NN Mn-pairs placed along [1-10] direction the lowest total energy is for the AFM spin configuration for the Mn-pair 10 & 14 in L(S)DA approach (indicated with green in Fig. 5) and for the Mn-pair 11 & 15 in L(S)DA+U approach (indicated with red in Fig. 5).

3. Reconstruction $\beta(2 \times 4)$

As in the previous sections, in the present one we discuss first structural and energetic properties of the Mn-dimers being the nearest neighbors and placed onto the $\beta(2 \times 4)$ reconstructed (001) surface.

Similarly like in the $\beta(2 \times 4)$ case, we start the discussion with a survey of possible placements of the Mn-pairs

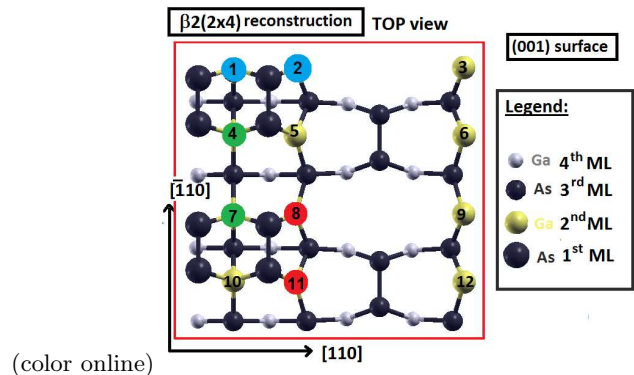


FIG. 6. Positions of the Mn-pair at the $\beta(2 \times 4)$ reconstructed surface. The most energetically favorable positions of the Mn-pair are indicated by the blue color (numbered 1 & 2, which is the same for both L(S)DA and L(S)DA+U approaches), and for the [1-10] crystallographic direction with green for L(S)DA (numbered 4 & 7) and with red for L(S)DA+U (numbered 8 & 11) schemes. The all other possible cationic positions where the Mn-atoms could be accommodated are indicated in yellow and also numbered. Positions of the As-atoms are denoted with big black dots and small grey dots, for the highest and deeper As-layers, respectively.

on the $\beta(2 \times 4)$ GaAs (001) surface. In the chosen symmetry of the supercell, the [110] and [1-10] directions are non-equivalent. Along the [110] crystallographic direction one can place the nearest neighbor Mn-pair on four equivalent ways on the cationic sublattice, such as 1 & 2, 4 & 5, 7 & 8, 10 & 11, whereas along the [1-10] direction on two equivalent ways which are 1 & 4, 7 & 10. However only along the [1-10] direction we can place Mn nearest neighbor pairs also in non-equivalent positions, such as 1 & 4, 2 & 5.

Concerning the distance between the Mn-atoms, our result show that the pairs with Mn-atoms being the nearest neighbors are energetically preferable in comparison of the configurations with larger distances between the Mn-atoms. In Tab. II we present the relative energy differences among all nearest neighbor class of Mn-dimer configurations, for two alignments of magnetic moments of the Mn-atoms (FM or AFM).

Among all NN Mn-pairs placed along [1-10] direction the lowest total energy is for the AFM spin configuration for both two approaches. However, for these two approaches the positions of the Mn-atoms are different, for the L(S)DA 4 & 7 (indicated with green in Fig. 6) and for the L(S)DA+U 8 & 11 (indicated with red in Fig. 6). In case of the Mn-pair along the [110] direction the ferromagnetic alignment of the Mn-spins are preferable.

As one can also see from Tab. II, the ground state of the Mn-pair on the $\beta(2 \times 4)$ reconstructed GaAs (001) surface is reached for the Mn-pair (with Mn-atoms being cationic nearest neighbors) and placed along [1-10] crystallographic direction with AFM aligned Mn-spins.

TABLE II. The ground state energies for all of the non-equivalent incorporations of the Mn-dimer at the nearest neighbor positions at the (001) $\beta 2(2 \times 4)$ surface. The Mn-pair positions are explained in Fig. 6. The displaced energies are the differences $\Delta E = E_{tot}^{slab, Mn}(MS) - E_{tot}^{slab, pure}$, given in eV per supercell. MS indicates the alignment of Mn magnetic moments, MS = FM, or AFM, and the $E_{tot}^{slab, pure} = -38570.17$ eV per supercell which contains 274 atoms. The results are obtained employing standard L(S)DA and L(S)DA+U (for $U = 4.5$ eV) approaches.

$\beta(2 \times 4)$ position	$\Delta E_{L(S)DA}$		$\Delta E_{L(S)DA+U}$ ($U = 4.5$ [eV])	
	E_{FM}	E_{AFM}	E_{FM}	E_{AFM}
[110] (1 & 2)	-733.684	-733.483	-739.621	-739.465
[1-10] (4 & 7)	-733.855	-733.892	-739.614	-739.552
[1-10] (5 & 8)	-733.483	-733.386	-739.530	-739.459
[1-10] (8 & 11)	-733.531	-733.571	-739.610	-739.693
[1-10] (7 & 10)	-733.825	-733.852	-739.601	-739.604

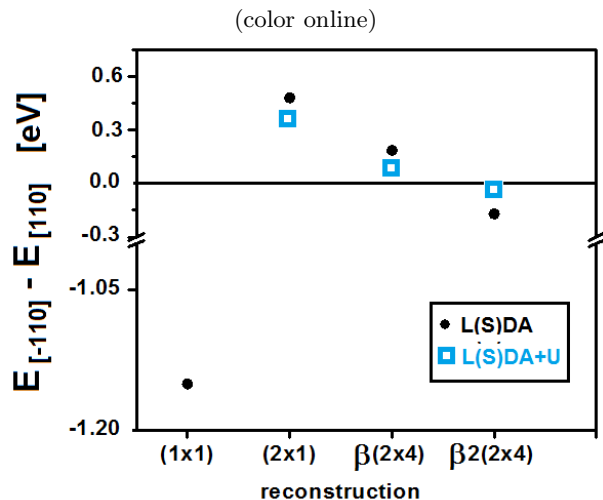


FIG. 7. Comparison of the most stable configurations of the Mn-pairs at surfaces with various reconstructions. The energy difference between the most stable NN configuration at [1-10] and [110] crystallographic directions, as obtained within the L(S)DA and L(S)DA+U schemes. The preferential orientation of the Mn-dimer depends on the surface reconstructions.

4. Comparison between different reconstructions

In this section, we make an attempt to generalize our theoretical studies presented in the previous sections and get physical understanding of the structural and energetic properties of surfaces decorated with Mn-pairs.

Our results show that the energy of the system strongly depends on the position, orientation, and the distance between the Mn-atoms. The Mn-pairs prefer to occupy the nearest neighbor positions (NN) independently on the reconstruction type at the surface. In other words they prefer to form dimers at the surface.

It turns out that for Mn-pairs with Mn-atoms being at the nearest neighbor distance, there are two crystal-

lographic orientation of Mn-dimers that lead to the energetic stability of the studied systems, namely the [110] and [1-10] crystallographic directions, as obtained within the L(S)DA and L(S)DA+U schemes. The energy difference, between the most stable configurations along the [1-10] and [110] directions are summarized for all considered surface reconstructions in Fig. 7. One can see that the energetically preferential orientation of the Mn-dimer depends on the surface reconstructions. In other words, it is plausible that during the growth process the Mn-ions would accommodate positions along the energetically preferential directions. The very recent measurements have shown that there exist the magnetic inhomogeneities on sub-millimeter length scales in GaMnAs samples [30], which can be assigned to anisotropic picture of Mn distribution. Moreover, our results have touched very important issue of the origin of the uniaxial magnetic anisotropy in (Ga,Mn)As samples. Recently, the authors have shown [4] that the preferential distribution of Mn-atoms at the surface is the physical origin of the symmetry breaking of the bulk GaAs crystal and consequently of the bulk uniaxial in-plane and out-of-plane magnetic anisotropies. Our results suggest that by changing the growth conditions (the reconstructions on the surface depend on it) one can design the direction of the magnetic easy axis in (Ga,Mn)As samples.

Furthermore, our results give also some hints how to change the preferential direction of the Mn-pairs at the surface, simply by changing the surface reconstructions through the choice of suitable growth conditions.

We have also demonstrated the importance of the relaxation of the atoms at the surface (see Fig. 3). The relaxation can change the preferential direction of Mn-dimer incorporation at the surface. In general, the relaxation of the atoms at the surface is larger for the Mn-pair along the [110] crystallographic direction than along the [1-10] one. Our results demonstrate also that the relaxations of the atoms are more pronounced at the surface than in the bulk crystal. Moreover, our results show that the magnetic interaction does not affect the energetically preferential incorporation

We also compare the stability of the pure surface with the stability of the just calculated surfaces with the incorporated Mn-dimers, which could mimic the surfaces of (Ga,Mn)As. To do this, we plot the surface free energy diagram versus the thermodynamically allowed range of the differences in the chemical potential of the atomic As and As bulk differences in Fig. 8. One can see that all the reconstructions concerned in Fig. 8 become more stable at the As-rich limit. While the $\beta 2(2 \times 4)$ -Mn[1-10] is found to be energetically the most favorable of all Mn-reconstructed surfaces considered in this paper. However, the difference in the energy in comparison with $\beta 2(2 \times 4)$ -Mn[1-10] and $\beta(2 \times 4)$ -Mn[110] is only 3 meV per \AA^2 . Moreover, the Mn-dimer incorporation into substitutional position at given reconstructed surface destabilize this surface by 55 meV/ \AA^2 - 59 meV/ \AA^2 . Recently, it has been theoretically predicted, that for the

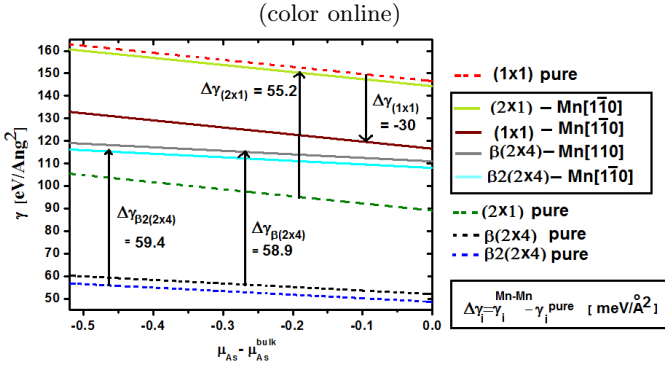


FIG. 8. Surface free energy diagrams for pure GaAs (001), As-terminated surface reconstructions: (1×1) , (2×1) , $\beta(2 \times 4)$, $\beta 2(2 \times 4)$ (denoted by the dashed lines), and for the most energetically preferable Mn-dimer substitutional incorporation onto these reconstructed surfaces (denoted by the straight lines) as predicted in this paper. Thermodynamically allowed range of the difference chemical potential of As and As-bulk is between -0.52 eV (Ga-rich conditions) and 0.00 eV (As-rich conditions). The arrows indicate the change in the surface free energy $\Delta\gamma_i$ between the given surface with Mn-dimer (γ_i^{Mn-Mn}) and the surface without the Mn (γ_i^{pure}). One can see that the Mn-dimer incorporation destabilizes the given pure reconstructed surface by $55 - 60$ meV/Å², except from the ideal (1×1) surface.

As-rich limit, the Mn-atoms are favorably incorporated into Ga-sites between the As-As dimer row in the $\zeta(4 \times 4)$ reconstructed surface[31] [7].

B. Magnetic and Electronic Properties

In this section, we first focus on the strength of the magnetic interaction of isolated Mn pairs. Then we examine the electronic structure and spin magnetic moments.

We start by considering all non-equivalent positions of Mn pairs (two Mn ions per cell), oriented along different crystalline directions and at various separations of Mn pairs, substituted onto cationic sublattice of Ga-atoms at the optimized reconstructed GaAs(001) surfaces, as it is shown as an example for (2×1) reconstructed surface in Fig. 9, where the position of one Mn atom is kept fixed (position 0 in Fig. 9), whereas the position of the second atom is varied along different crystallographic directions at the (001) surface.

In order to show how the strength of the magnetic interaction of the Mn ions changes with the Mn-Mn separation length, we plot the absolute value of energy difference between AFM i FM alignment of the magnetic moments of Mn-atoms as a function of their separation (see Fig. 10). We assume collinear magnetic configurations of Mn ions in which magnetic moments are either parallel or antiparallel. We do not include spin-orbit interaction, because it has been reported recently, that the

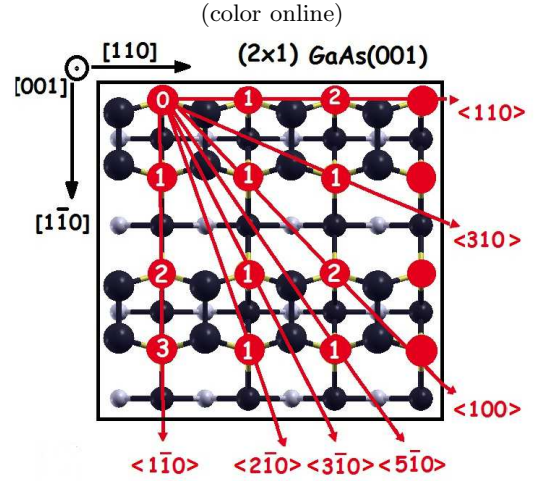


FIG. 9. All non-equivalent positions of Mn pair on the (2×1) reconstructed (001) surface. The two Mn-atoms, replacing Ga-atoms (red spheres), are marked 0 (first Mn-atom) and 1,2,3 (second Mn-atom), e.g. 0-3 [1-10] denotes that the Mn pair is along [1-10] crystallographic direction, where Mn-atoms constituting the pair sit on 0 and 3 position as is depicted on panel (A). All equivalent symmetry directions $\langle \dots \rangle$ have been chosen in direct cubic coordinates [...], in such a way that all Mn pairs appear in (001) plane. Positions of the atoms in the uppermost monolayers are indicated by larger symbols.

SOI have a small influence on exchange coupling J (few meV) [10][32].

Since the exchange interaction is a crucial quantity in the field of DMS, we start our discussion in comparison of our results with the other theoretical predictions taken from literature [9, 10, 20, 30] (see Fig. 10), for both bulk and surface calculations obtained within different methods and different concentration of Mn ions.

The general trends of the exchange energy for both surface and bulk calculations are similar. These results show strong anisotropic character of the exchange energy versus the distance between the Mn pair, and a decay of the magnetic interaction with increasing distance between the magnetic ions. The largest exchange energies are observed for the smallest separation of the Mn-atoms independently of the method and a system used. The strong exchange interaction are in particular importance in case of its successful applications in spintronic devices, therefore further in this paper we present the detail discussion about the exchange interaction of the all possible nearest neighbours NN positions at chosen reconstructed (001) GaAs surfaces.

The main difference between our and previously reported results is that we obtain anisotropic character not only for the different length between magnetic atoms, but even for the given separation distance (without taken into account spin-orbit interaction SOI), which have not been pointed before for surface studies. Only Strandberg et al. [9], which take into account the SOI, pointed out the

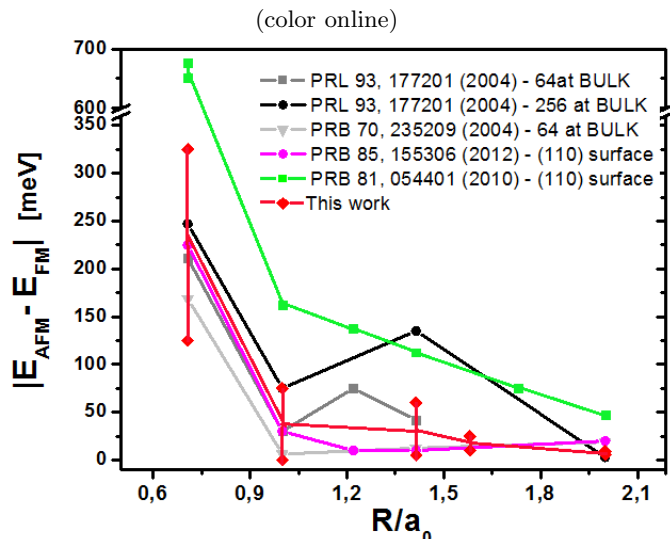


FIG. 10. The absolute value of the total energy difference between ferromagnetic and antiferromagnetic orientation of two Mn-spins as a function of Mn-Mn separation (in lattice constant units a_0) for the isolated pair, for the surface and bulk calculations. The red line presents the result of this work for the surface reconstruction (2×1) , and the red vertical lines indicate the obtained range of the magnetic energies for all of the non-equivalent directions of the Mn-pair but for the given separation between the Mn-ions obtained in this work. The rest of the result are taken from literature.

difference of around 13 meV between two non-equivalent positions of the NN pairs [33]. In our calculations the changes are around hundredths of meV. This is the result of taking into account reconstructed surfaces, which enters another possibilities of placement of Mn ions at given distance between them. We will discuss this effect in more details below.

1. Effective exchange coupling

To quantify the strength of the magnetic coupling between two Mn ions at NN position, we have analyzed the the effective exchange constant $J(r_{ij})$ for the all non-equivalent NN distance between the Mn ions at reconstructed surfaces GaAs (001): (2×1) , $\beta(2 \times 4)$, and $\beta 2(2 \times 4)$ (see Tab. III), according to the formula: $J = (E_{AFM} - E_{FM}) / (2 * (5/2)^2)$. Here we assume the spin magnetic moments of $5/2$.

Our results clearly demonstrate that the Mn dimer along [110] crystallographic direction exhibits ferromagnetic alignment of spins (positive values of the exchange coupling J , see Tab. III) with magnetization vectors on each Mn-atom being oriented along the [001] direction and of magnitude equal to $4.7 \mu_B$, independently of the type of reconstructed surface. For the dimer along [1-10] crystallographic direction, the anti-ferromagnetic alignment of the spins is mostly likely to appear (mostly neg-

TABLE III. The exchange coupling J given in eV for the nearest neighbor Mn-pairs for various considered reconstructed surfaces. The numbers in brackets are the obtained range of the exchange coupling. The results are obtained employing standard L(S)DA and L(S)DA+U (for $U = 4.5$ eV) approaches.

J [eV]	reconstructed surface (001)		
	(2×1)	$\beta(2 \times 4)$	$\beta 2(2 \times 4)$
Mn-Mn pair along [110]			
L(S)DA	+0.012	(+0.010,+0.024)	+0.016
L(S)DA+U	+0.008	(+0.008,+0.019)	+0.012
Mn-Mn pair along [1-10]			
L(S)DA	(-0.030,-0.024)	(-0.001,+0.010)	(-0.003,+0.008)
L(S)DA+U	(-0.044,-0.036)	(-0.007,+0.001)	(-0.005,+0.006)

ative values of the exchange coupling J , see Tab. III). In other words, the mechanism of the magnetic ordering has the anisotropic character, namely it depends on the Mn pair orientation. This rises a question whether it would be possible (e.g., by the STM method) to incorporate on purpose the magnetic atoms along a given direction at the surface. Then one could obtain on purpose magnetic or non-magnetic material. One can see that the value of the exchange constant for a given orientation of Mn dimer depends on the type of surface reconstruction, indicating that the exchange constant depends sensitively on the lattice arrangement of the atoms.

Now we attempt to compare our result with the exchange coupling for the dimer reported so far in the literature. These reports show that the effective J for the dimer is highly sensitive to doping levels and increases with decreasing Mn concentration [20, 30, 34, 35]. The order of magnitude of the exchange coupling is the same as previously reported for the surface and bulk results. The bulk calculations always predict the ferromagnetic ordering of the Mn-spins.

In case of the surface results, as it has been mentioned before in this paper, only the unreconstructed non-polar GaAs (110) surface has been considered. The M. Fhokrul Islam *et al.* [10] in the framework of DFT in GGA approach obtained the value equal to 17.9 meV[36] for the nearest neighbour configuration. Strandberg *et al.* [9] studied the pairs of Mn ions at the surface. They obtained positive values of J for two different directions of Mn-dimer at the (110) surface, 54 meV and 53 meV, for the very low Mn concentration of $x = 0.0006$. They used the kinetic tight binding model. Due to the restrictions of the model they did not take into account relaxations of the atoms at the surface. This can significantly influence the obtained results. Therefore, we believe that our results are correct and the different ordering mechanism is related with the position and the relaxations of the atoms. We will try to prove it below.

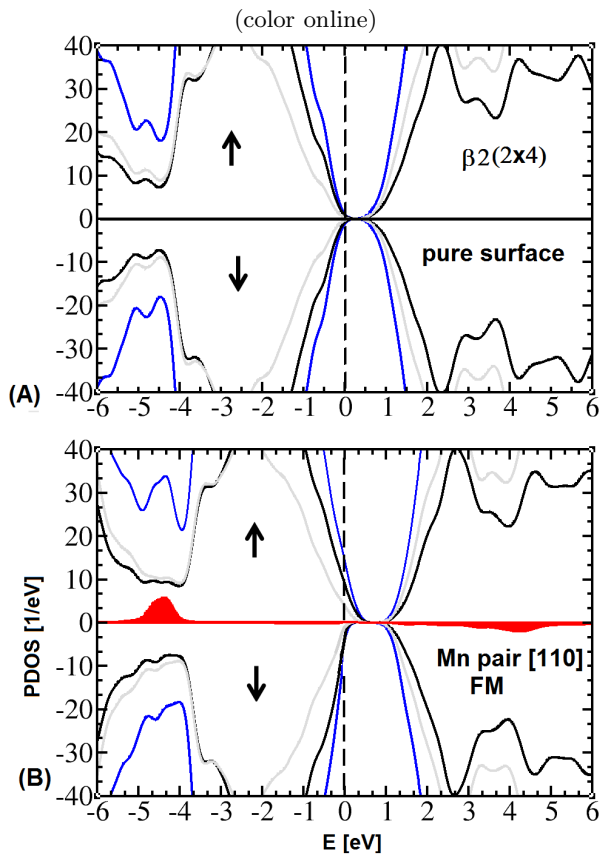


FIG. 11. Projected DOS calculated within L(S)DA+U method for: (A) pure $\beta 2(2 \times 4)$, and (B) the Mn-dimer substituted onto cationic sublattice along $[110]$ crystallographic direction at the $\beta 2(2 \times 4)$ surface. The pure $\beta 2(2 \times 4)$ surface is semiconducting, whereas substituted Mn-ions introduce extra states above the Fermi level within the valence band. The vertical dashed line denotes the position of the Fermi level. The solid blue, black, and grey lines correspond respectively to total density of all states in a system, total density of As-states, and total density of Ga-states. The red area is the contribution from Mn d states. The positive values of PDOS represent spin-up channel (negative -spin-down).

2. Electronic structure and spin magnetic moments

The pure (2×1) surface is metallic and the surface states are placed in the bandgap of the bulk, whereas the pure β -surfaces are semiconducting (see Fig. 11(A)) and do not introduce the surface states into the bulk's gap. When the two Ga ions are substituted by the Mn ions, the extra electronic states appear just above the Fermi level (see Fig. 11(B) and Fig. 14). These empty states which are above the Fermi level and belong to the valence band can be identified with the acceptor hole states. As hole states we consider unoccupied states with energies between Fermi energy (lying in the valence band)[37] and top of the valence band, as it was previously considered for a bulk system [38, 39]. The hole states have mostly p character (see Fig. 12(A)).

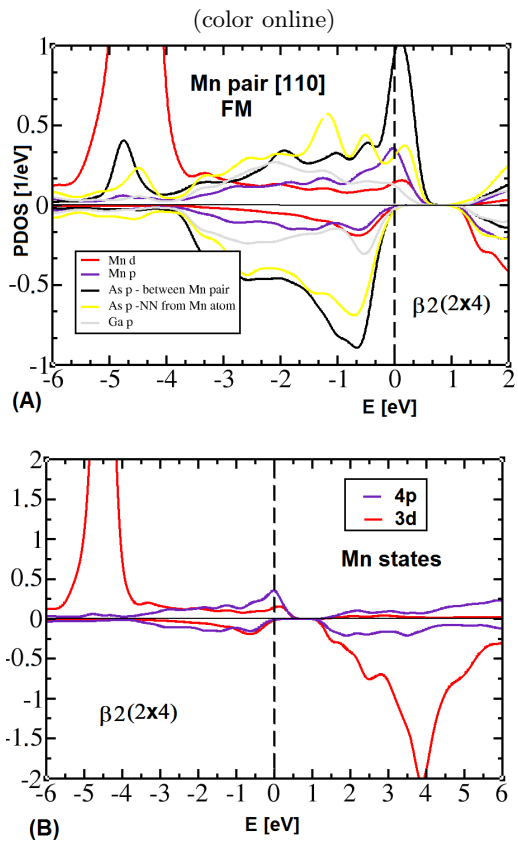


FIG. 12. PDOS for the Mn-pair at the reconstructed $\beta 2(2 \times 4)$ surface. Projected density of states as obtained from the L(S)DA+U calculations for: (A) the surrounding atoms of the Mn-dimer along the $[110]$ crystallographic direction, and (B) the comparison between the Mn p and d states.

The greatest contribution to the holes comes from the arsenic atoms, which are the nearest neighbors of the Mn pair and reside along the $[110]$ crystallographic direction (see Fig. 12(A)). Moreover, the $3d$ states are mainly localised around 4.5 eV below the Fermi level (see Fig. 12(B)). Therefore, the Mn p states hybridize with the surrounding stronger than the $3d$ states. There is only small admixture of the Mn d -states with the hole states.

Now let us discuss the spatial distribution of the hole, in order to visualize its character.

The hole occupation is defined here as the integral over energy of the density of states from the Fermi energy to the top of the valence band, N_h . Note that the same procedure were previously adopted in Refs. [38] and [39], and calculated for a bulk system. One can also consider integrated density of states $N_{h,layer}$ coming from the projected DOS for various slab layers, and even atoms within the layers $N_{h,layer}^{atom}$. The analysis of the contribution of these layer and atomic states to the total hole density (N_h) defined above is presented in Fig. 13(A) and 13(C) in case of the $\beta 2(2 \times 4)$ reconstructed surface, respectively. Similar results we have also obtained for $\beta 2(2 \times 4)$ recon-

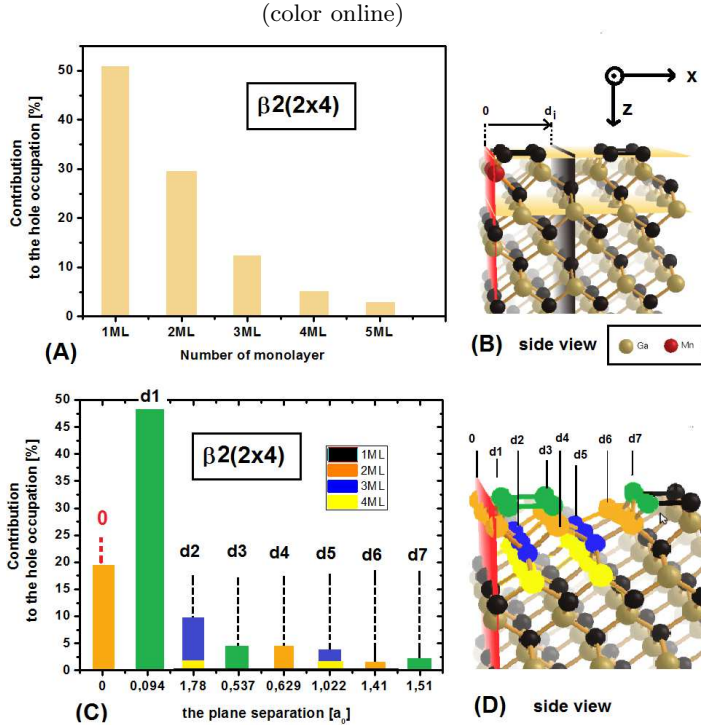


FIG. 13. Distribution of the holes for $\beta 2(2 \times 4)$ reconstructed surface. (A) Sum of the orbital contributions to the hole occupations [in %] from atoms residing on the different monolayers. 1ML, 2ML etc. indicate the monolayer plane counted down from the top of the slab, i.e., with increasing z -component. The black d_i plane is parallel to the red plane where the Mn-atoms reside. (B) The coordinate system with origin on the top of the slab. The black and red planes are (100) planes, the orange planes are (001) ones. (C) Orbital contributions to the hole occupation coming from the atoms lying on the cross sections of the (100) and (001) planes. d_0, d_1, d_2 etc., indicate the x -coordinates of these lines, whereas the green, orange, blue and yellow colors indicate the z -coordinate; as illustrated in the panel (D). The Mn-atoms reside on the 2ML.

struction. The orbital contributions to the hole states decrease with the number of the monolayers (see Fig. 13(A)).

Moreover, the contributions to the hole occupation coming from the atoms at each d_i plane decrease rapidly with its distance from the plane where the Mn-atoms sit (see Fig. 13(C)). Nevertheless, the small contributions from distant atoms are visible, just indicating extensive spatial delocalisation of the holes. The delocalisation of the holes is a factor which is favorable for the mediation of the exchange interaction between the Ga-atoms and, therefore, for higher Curie temperature.

Although, we have demonstrated that the holes have extended character over many atoms from the Mn-dimer, in comparison to the bulk calculations [38, 39], the holes states are more localised around the Mn-pair. In the bulk calculations, the hole extends over the first and second

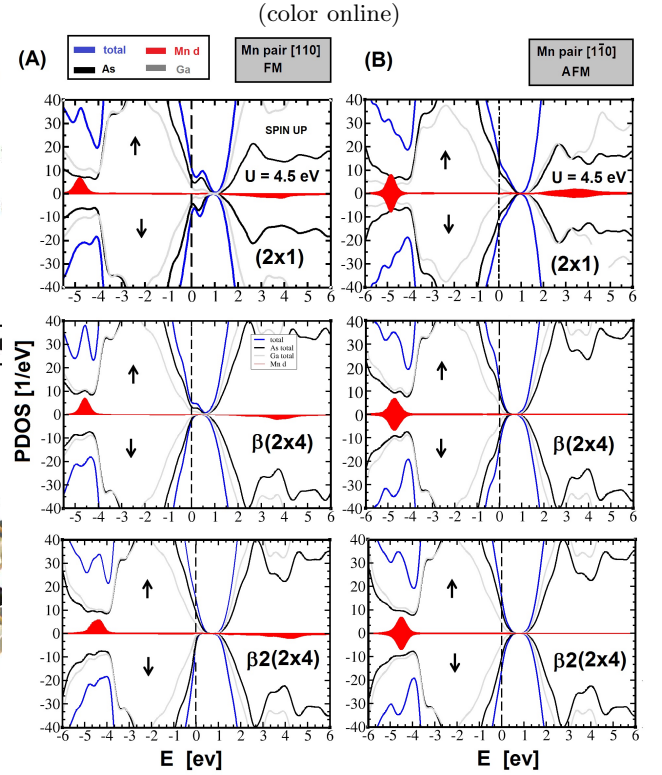


FIG. 14. Comparison of the PDOS of the two Mn dimer orientation: [110] (left side of the picture) and [1-10] (right side of the picture) for a different surface reconstructions: (2×1) , $\beta(2 \times 4)$, $\beta 2(2 \times 4)$. The vertical dashed line denotes the position of the Fermi level. The solid blue, black, and grey lines correspond respectively to total density of all states in a system, total density of As-states, and total density of Ga states. The red area is the contribution from Mn d states.

coordination spheres of As- and Ga-atoms [38, 39].

Another noteworthy finding is that there is no formation of impurity band on the surface. This situation clearly corresponds to the Zener type (or RKKY one) [40] of magnetic coupling between Mn ions, and one can talk about surface, ligand-ion, $p-d$ interaction.

In the case of the Mn-pair along the [1-10] direction, the Mn prefer to be anti-ferromagnetically aligned with respect to each other. After the geometry optimization the Mn-As-Mn angle increases by the 11° - 16° depending on the reconstruction used, making the angle to be equal to 119° - 122° . The relaxation of the atoms are presented in Fig. 15 for the (2×1) reconstructed surface. This feature can be explained in terms of the the so-called Goodenough-Kanamori-Anderson rules. According to these rules, a superexchange is anti-ferromagnetic when the angle of magnetic ion-ligand-magnetic ion angle is 180° , whereas angle close to 90° prefers the ferromagnetic ordering mechanism.

Now let us change our attention to the spin magnetic moments, by using a Mulliken analysis [41]. Our results clearly show that the local magnetic moments of Mn-ions polarize their surrounding always in such a way,

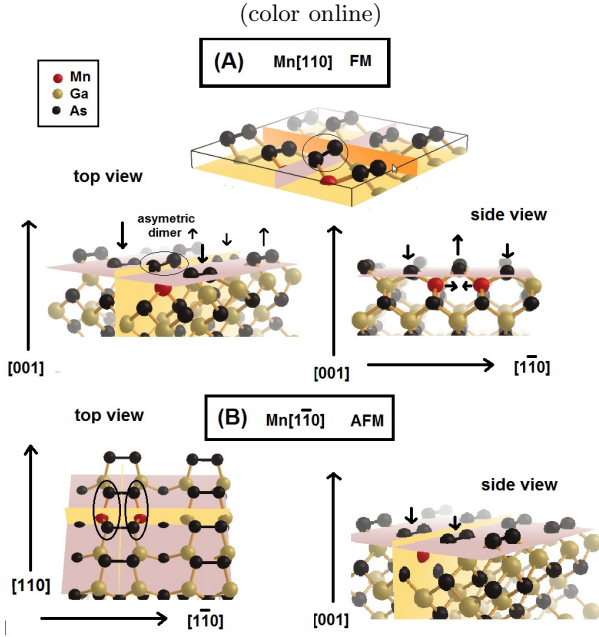


FIG. 15. Relaxation of the atoms at the (2×1) surface. - The optimized structure of the Mn-pair along $[110]$ direction for: (A) FM and (B) AMF alignment of the Mn-spins. After optimization the asymmetric dimer appears at the surface between the Mn-pair for both Mn-spins directions. The arrows above the atoms indicate the directions of the atoms' relaxation. Note, that there is opposite character of relaxation of two different alignment of Mn-spins (FM or AFM). Namely, for ferromagnetically aligned spins, the distance between the Mn-atoms decreases by about 0.18\AA after optimization, whereas the As-atom which links the Mn-pair relaxes outward the surface by about 0.3\AA in the $[001]$ direction. All of the distance changes given here are relative to the distances at the pure (2×1) surface. In the case of AFM spins (B), the Mn-pair distance increases by about 0.31\AA , and hence the As-atom which links the Mn-pair relaxes inward the bulk. As a consequence, the angle between the Mn-pair and its linking As-atom increases after optimization and becomes more planar. The local changes near the Mn-pair induce the changes at the whole surface for both spins directions. The similar behaviour is observed for the $\beta(2 \times 4)$ and $\beta 2(2 \times 4)$

that the nearest neighbor As-atom acquires the magnetic moments anti-ferromagnetically aligned to the Mn-spins, which is schematically illustrated in Fig. 16. In the case of Mn-pair at $[110]$ direction, the contributions coming from the surrounding atoms are listed and compared for different reconstructions in Tab. IV. One can see that the induced magnetizations are comparable and do not depend on the type of reconstructed surfaces. The induced magnetic moments decrease rapidly with the increasing distance to the Mn-pair. The nearest neighbors of the Mn-pair have only noticeable induced spin polarization, for the second neighbors they are smaller than $0.01 \mu_B$, and for the third ones are nearly equal to zero. This picture emerges from both L(S)DA and L(S)DA+U calculations. In the bulk system, on the first, second,

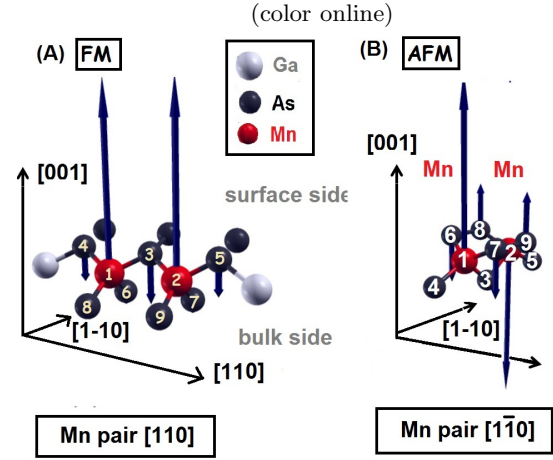


FIG. 16. Illustration of the magnetic moments for the (2×1) reconstructed surface. Magnetic moments on the Mn-atoms and in their neighborhood for the Mn-pair along $[110]$ direction at the surface and for two arrangements of Mn-spins: the FM (A) and AFM (B). The blue arrows indicate schematic distribution of the magnetic vectors. The lengths of the magnetic vectors on As-sites are exaggerated for clarity of the presentation.

TABLE IV. The spin magnetic polarization of the As-atoms surrounding Mn-ions for the FM arrangement of Mn-pair at $[110]$ direction for various reconstructed surfaces, calculated by using a Mulliken analysis [41]. The integers in the subscript indicate the position of the atom at the surface which is explained in Fig. 16.

atom	(2×1)	$\beta(2 \times 4)$	$\beta 2(2 \times 4)$
As ₃	-0.74	-0.75	-0.79
As ₄	-0.2	-0.17	-0.2
As ₅	-0.2	-0.17	-
As ₉ =As ₇	-0.12	-0.10	-0.17
As ₈ =As ₆	-0.12	-0.10	-0.09

and third Mn neighbor extends to $0.11 \mu_B$, $0.015 \mu_B$, and $0.015 \mu_B$, respectively (according to the L(S)DA+U results from [20]). This comparison between the bulk and the surface shows that the induced magnetic moments are more confined at the surface than in the bulk. In addition, the induced magnetic moments on the atoms depend on atomic positions in the slab. They are always larger at the surface than at the monolayer closer to the bulk site. This picture emerges from both L(S)DA and L(S)DA+U calculations. In the case of AFM alignment of Mn-spins, the As-atom in between the Mn dimer is not spin polarized (see Fig. 16 (B)), whereas the closer neighbors of Mn-atoms have similar absolute values of spin polarization like in the FM case.

IV. CONCLUSIONS

We have studied the Mn-pairs substituted onto Ga sublattice at different As-terminated reconstructed GaAs (001) surfaces. We have demonstrated that the energy of the system strongly depends on the position, orientation, and the distance between the Mn-atoms. The most preferential energetically position of Mn-pair is the nearest neighbor position (NN, Mn-dimer), independently of the reconstruction pattern studied in this paper. We have shown that there are only two crystallographic orientation of the Mn-dimer: [110] and [1-10], which are energetically non-equivalent at the surface. In the case of the (2×1) and $\beta(2 \times 4)$, the Mn-dimer along [110] direction is more preferable, whereas for the (1×1) and $\beta 2(2 \times 4)$ the Mn-dimer along [1-10] is favorable. Our results give a clue how to change the magnetic anisotropy of the (Ga,Mn)As layer [1], simply by changing the reconstructions at the semiconductor surfaces, which can be done by changing the growth conditions, such as the vapour, temperature or surface composition [42, 43].

Moreover, we have demonstrated that the mechanism of the magnetic ordering depends on the Mn-pair orientation. Generally, the Mn-dimer along [110] crystallographic direction exhibits ferromagnetic alignment of the spins, whereas the Mn-dimer along [1-10] crystallographic direction prefers to be anti-ferromagnetically aligned. The latter can be understood in terms of the

Goodenough-Kanamori-Anderson rules. In addition, we have shown that the Mn $4p$ states have greater contribution to the hole states than $3d$ states, which is consistent with recently published theoretical results for bulk [38, 39].

We have demonstrated that the holes are mostly localised in the closest proximity of the Mn-pair. Nevertheless, there are small contributions which come from the distant atoms indicating extended character of the holes. All this strongly suggest that the Zener $p - d$ interaction [40] can also cause ferromagnetic coupling of the Mn-pairs at the surface.

Furthermore, our results clearly show that the local magnetic moments of Mn-ions polarize their surrounding always in such a way, that the nearest neighbor As-atom acquires the magnetic moments anti-ferromagnetically aligned to the Mn-spins.

ACKNOWLEDGMENTS

This work was supported by the European Research Council through the FunDMS Advanced Grant within the "Ideas" Seventh Framework Programme of the EC and InTechFun (POIG.01.03.01-00-159/08) of EC. We made use of computing facilities of PL-Grid Polish Infrastructure for Supporting Computational Science in the European Research Space, and acknowledge the access to the computing facilities of the Interdisciplinary Centre of Modelling, University of Warsaw.

-
- [1] M. Birowska, C. Śliwa, J. A. Majewski, and T. Dietl, *Phys. Rev. Lett.* **108**, 237203 (2012).
 - [2] D. Chiba, M. Sawicki, Y. Nishitani, F. Matsukura, and H. Ohno, *Nature* **455**, 515 (2008).
 - [3] D. Kitchen, A. Richardella, J.-M. Tang, M. E. Flatte, and A. Yazdani, *Nature* **442**, 436 (2006).
 - [4] H. Fu, L. Ye, K. Zhang, and X. Xie, *Surface Science* **341**, 273 (1995).
 - [5] S. C. Erwin and A. G. Petukhov, *Phys. Rev. Lett.* **89**, 227201 (2002).
 - [6] S. B. Zhang, L. Zhang, L. Xu, E. G. Wang, X. Liu, J.-F. Jia, and Q.-K. Xue, *Phys. Rev. B* **69**, 121308 (2004).
 - [7] A. Ohtake, A. Hagiwara, and J. Nakamura, *Phys. Rev. B* **87**, 165301 (2013).
 - [8] P. Mahadevan and A. Zunger, *Phys. Rev. B* **68**, 075202 (2003).
 - [9] T. O. Strandberg, C. M. Canali, and A. H. MacDonald, *Phys. Rev. B* **81**, 054401 (2010).
 - [10] M. F. Islam and C. M. Canali, *Phys. Rev. B* **85**, 155306 (2012).
 - [11] P. Hohenberg and W. Kohn, *Phys. Rev.* **136**, B864 (1964).
 - [12] W. Kohn and L. J. Sham, *Phys. Rev.* **140**, A1133 (1965).
 - [13] D. M. Ceperley and B. J. Alder, *Phys. Rev. Lett.* **45**, 566 (1980).
 - [14] P. Ordejón, E. Artacho, and J. M. Soler, *Phys. Rev. B* **53**, R10441 (1996).
 - [15] N. Troullier and J. L. Martins, *Phys. Rev. B* **43**, 1993 (1991).
 - [16] S. G. Louie, S. Froyen, and M. L. Cohen, *Phys. Rev. B* **26**, 1738 (1982).
 - [17] E. Artacho, D. Sánchez-Portal, P. Ordejón, A. García, and J. M. Soler, *physica status solidi (b)* **215**, 809 (1999).
 - [18] J. Okabayashi, A. Kimura, O. Rader, T. Mizokawa, A. Fujimori, T. Hayashi, and M. Tanaka, *Phys. Rev. B* **64**, 125304 (2001).
 - [19] T. Jungwirth, J. Sinova, J. Maš, J. Kučera, and A. H. MacDonald, *Rev. Mod. Phys.* **78**, 809 (2006).
 - [20] M. Wierzbowska, D. Sánchez-Portal, and S. Sanvito, *Phys. Rev. B* **70**, 235209 (2004).
 - [21] D. A. Murdick, X. W. Zhou, H. N. G. Wadley, and D. Nguyen-Manh, *Journal of Physics: Condensed Matter* **17**, 6123 (2005).
 - [22] O. Madelung, *Semiconductors: Data Handbook, 3rd ed.* (Springer, Berlin, 2004).
 - [23] M. D. Pashley, K. W. Haberern, W. Friday, J. M. Woodall, and P. D. Kirchner, *Phys. Rev. Lett.* **60**, 2176 (1988).
 - [24] E. J. Heller and M. G. Lagally, *Applied Physics Letters* **60**, 2675 (1992).
 - [25] M. Gallagher, R. Prince, and R. Willis, *Surface Science* **275**, 31 (1992).
 - [26] A. Avery, D. Homes, J. Sudijono, T. Jones, and B. Joyce, *Surface Science* **323**, 91 (1995).

- [27] M. Takahasi, Y. Yoneda, N. Yamamoto, and J. Mizuki, *Phys. Rev. B* **68**, 085321 (2003).
- [28] Experimentally, this reconstruction is observed on Si(001) surfaces.
- [29] S. Colonna, E. Placidi, F. Ronci, A. Cricenti, F. Arciprete, and A. Balzarotti, *Journal of Applied Physics* **109**, (2011).
- [30] P. Mahadevan, A. Zunger, and D. D. Sarma, *Phys. Rev. Lett.* **93**, 177201 (2004).
- [31] This reconstruction has not been considered in these calculations.
- [32] We have tested the accuracy of calculations with SOI included. Our results show extremely high accuracy needed to obtain reliable surface results, for such big supercells that properly simulate the diluted case.
- [33] Taken from the Fig. 14 [9] for the $0.707 R/a_0$ the effective exchange coupling is around 1 meV, whereas the exchange energy is $1 \text{ meV} \times 2 \times (5/2)^2$.
- [34] M. v. Schilfgaarde and O. N. Mryasov, *Phys. Rev. B* **63**, 233205 (2001).
- [35] J. Kudrnovský, I. Turek, V. Drchal, F. Mácá, P. Weinberger, and P. Bruno, *Phys. Rev. B* **69**, 115208 (2004).
- [36] In the paper [10] see Table VII. for $U = 4 \text{ eV}$ the value is 223.7. In order to compare our results with them we divided their value by 12.5.
- [37] We want to make a comment here. We have not considered the holes in the system with Mn pair on the (2×1) reconstructed surface. The reason of that is due to the appearance of the unoccupied surface states in the bandgap for the pure (2×1) reconstruction, and their mixing with the unoccupied states coming from the substitution of the Mn-atoms at cationic sublattice.
- [38] L. M. Sandratskii, P. Bruno, and J. Kudrnovský, *Phys. Rev. B* **69**, 195203 (2004).
- [39] K. Z. Milowska and M. Wierzbowska, *Chemical Physics* **430**, 7 (2014).
- [40] T. Dietl, F. Matsukura, J. Cibert, and D. Ferrand, *Science* **287**, 1019 (2000).
- [41] R. S. Mulliken, *J. Chem. Phys.* **23**, 1833 (1955).
- [42] H. Shimizu, T. Hayashi, T. Nishinaga, and M. Tanaka, *Applied Physics Letters* **74**, 398 (1999).
- [43] G. M. Schott, W. Faschinger, and L. W. Molenkamp, *Applied Physics Letters* **79**, 1807 (2001).